Applied Radiation and Isotopes 229 (2026) 112412

Contents lists available at ScienceDirect

Applied Radiation and Isotopes

journal homepage: www.elsevier.com/locate/apradiso

A radiometric and elemental characterisation of sludge and scales found in Dutch geothermal plants

Linde Pollet [a,b,*], Mikael Hult [a], Mirela Vasile [c], Gerd Marissens [a], Heiko Stroh [a], Sonja Schreurs [b], Wouter Schroeyers [b]

[a] European Commission, Joint Research Centre (JRC), Retieseweg 111, 2440, Geel, Belgium
[b] Hasselt University, CMK, research group NuTeC, Agoralaan building H, 3590, Diepenbeek, Belgium
[c] SCK.CEN, Boeretang 190, 2400, Mol, Belgium

ARTICLE INFO

Keywords:
Geothermal industry
Naturally occurring radionuclides
Radiation risk

ABSTRACT

Geothermal energy originates from the heat stored within the Earth's core. Thermal water from geological reservoirs is extracted to the surface to generate electricity or heat buildings and greenhouses. This thermal water contains various dissolved solids that can deposit, precipitate, and form scales in the installations as the water is brought to the surface. The dissolved solids contain primordial radionuclides. Workers are exposed to these radionuclides while maintaining and cleaning geothermal plants.

This study complements the limited research available on naturally occurring radionuclides in geothermal installations by examining their presence in various facilities across the Netherlands. Sludge and scale samples were provided from five different surface installations. The samples were analysed using radiometric methods (alpha-particle and gamma-ray spectrometry) and a non-radiometric method (energy dispersive X-ray fluorescence, EDXRF). EDXRF identified several hazardous elements, such as Lead, Arsenic, Chromium, and Thallium. In the scales, radiometric analysis detected three main radionuclides: ^{228}Th, ^{210}Pb, and ^{210}Po. Furthermore, for both scales and sludges, a notable disruption in the equilibrium was observed in parts of the natural decay chains ^{232}Th-^{228}Ra-^{228}Th and ^{226}Ra-^{210}Pb-^{210}Po, complicating the correct assessment of the massic activity of the radionuclides and the appropriate disposal of the materials. These findings highlight the importance of mapping Naturally Occurring Radioactive Materials (NORM) during geothermal plant maintenance and accurately assessing their massic activity.

1. Introduction

Geothermal energy is an energy source that uses the heat provided by the Earth's core. It is considered environmentally friendly as its greenhouse gas emissions are very low compared to energy based on fossil fuels. Furthermore, the technical installations occupy a much smaller area than many other energy generation forms. The primary advantage of geothermal energy lies in its abundant and reliable heat source. It is a fundamental energy source independent of weather conditions that can provide heat continuously in the long term (Palomo-Torrejón et al., 2021). For example, in 2015, the Netherlands produced 790 MW of thermal power and generated 6426 TJ/year of energy, whereas 70300 MWth of power and 587800 TJ/year were generated worldwide (Bertani, 2016).

In most geothermal installations, thermal water from geological reservoirs is extracted to the surface to generate electricity or heat buildings and greenhouses. During the pumping process, dissolved solids such as aluminium, copper, Iron and heavy metals like lead are carried along with the geothermal water from the reservoir (Gallup, 1997), (Regenspurg et al., 2010), potentially accumulating in the installation as scales or sludge since their solubility changes with variations in pressure, temperature and redox conditions. This accumulation reduces water flow and decreases heat transfer efficiency in heat exchangers. To prevent (acute) clogging of heat exchangers and pumps, bag and candle filters are integrated into circuits to capture the majority of the accumulating particles. These filters need to be changed regularly with intervals depending on the properties of the thermal water (Mahler et al., 2013), (Mathiesen et al., 2021).

Thermal waters often contain Naturally Occurring Radionuclides (NORs) and, related to their natural discharge in the form of thermal

* Corresponding author. European Commission, Joint Research Centre (JRC), Retieseweg 111, 2440, Geel, Belgium.
E-mail address: linde.pollet@uhasselt.be (L. Pollet).

https://doi.org/10.1016/j.apradiso.2025.112412
Received 27 June 2025; Received in revised form 25 October 2025; Accepted 30 December 2025
Available online 30 December 2025

springs, mineral precipitates can form due to the changing physico-chemical conditions, which can accumulate these radionuclides (Eross et al., 2012), (Kovács-Bodor et al., 2019). Subsequently, NORs have also been detected in the geothermal reservoirs both through drillings and from the pumped geothermal water (Kölbel et al., 2020), (Kölbel et al., 2021), (Tomaszewska and Bodzek, 2013), (Rihs et al., 1997), (Vasile et al., 2017), (Regenspurg et al., 2014). NORs are known to accumulate in the circuits, getting trapped in the filters and precipitating on surfaces (Pauwels et al., 2021).

NORs exhibit chemical properties identical to their corresponding stable isotopes and, to a certain extent, are similar to the elements in the periodic table that are grouped in the same column. This similarity is due to the elements in a family having the same number of valence electrons that are primarily responsible for the element's chemical behaviour. Consequently, the Group 1 alkali metals Li-Na-K-Rb-Cs-Fr are highly soluble in water. The solubility of Group 2 alkaline earth metals Be-Mg-Ca-Sr-Ba-Ra increases with increasing atomic number. As moving groundwater interacts with the rock formation along the flow path, resulting in a changing geochemical environment and because of the different chemical behaviour of elements (of different groups), it is expected to find radioactive disequilibria in the natural decay chains in geothermal fluids as long-lived daughters like ^{228}Ra and ^{228}Th have time to react chemically before they disintegrate. Compared to lead and thorium, radium is more soluble and easily mobilised due to high Cl concentrations and high content of dissolved material of geothermal fluids (Mathews et al., 2018). In addition, radium isotopes (^{223}Ra, ^{224}Ra, ^{226}Ra and ^{228}Ra) undergo recoil following alpha-decay of the parent radionuclides. At the surface of the mineral grains, the recoil enhances the probability of Ra-isotopes being released into the thermal water (Eggeling et al., 2013). On the other hand, uranium and thorium are not likely to be found in the thermal water as they will predominantly occur in their reduced and relatively immobile oxidation states U(IV) and Th (IV), owing to the reducing conditions (Regenspurg et al., 2014), (Zhang et al., 2014), (Harmsen and de Haan, 1980).

Due to the presence of NORs, workers are exposed to radiation when handling certain materials in geothermal plants (Shinonaga et al., 2023). According to the Euratom Basic Safety Standards (Council of the European Union, 2014), these materials can often be classified as Naturally Occurring Radioactive Materials (NORM). There are several reports related to the measurements of scales and filters with predominantly the following radionuclides: ^{238}U, ^{226}Ra, ^{210}Pb, ^{228}Ra, ^{228}Th, and ^{40}K (Regenspurg et al., 2014), (Pauwels et al., 2021), (Eggeling et al., 2013). However, due to the significant variation in geothermal formations' chemical and mineral content, a more thorough understanding of the radiological impact on geothermal plants requires more studies. It is worth pointing out that detailed studies regarding radiation exposure to workers of such facilities are very scarce. This fact was emphasised via a stakeholder analysis at the recent Ricomet 2023 workshop (Perko and Geysmans, 2023). Due to insufficient systematic research on NOR accumulation during geothermal energy production, it is currently challenging to predict, after an initial prospection of the geothermal reservoir, whether a geothermal installation will face significant NOR accumulation or if the radionuclide content of the residues falls below the exemption limit (Perko and Geysmans, 2023). This uncertainty impacts the cost of companies' waste disposal. The industrial use of geothermal heat for generating electricity and providing thermal heating to districts is still in its early stages, with limited scientific studies. This indicates the necessity for further characterisation and dissemination of information throughout the scientific community.

Consequently, this study aims to enhance understanding of the increased concentrations of natural radioactivity found in sludges and scales encountered in geothermal surface installations, marking this the first application to these installations in the Netherlands. By focusing on these by-products, the research emphasises the challenges of radiometric characteristics, the disruption of equilibrium in the natural decay chains, potential environmental impacts, and implications for worker safety. Additionally, it seeks to provide valuable data that can inform regulatory frameworks and optimise waste management practices within the geothermal energy sector.

2. Materials and methods

2.1. Site description

The data presented in this paper originate from four geothermal installations located in the South Holland region and one in Brabant, the Netherlands. The thermal reservoirs of all these facilities are located in a sandstone formation. The installations operate at relatively low temperatures (50 °C–60 °C) and supply heat directly to greenhouses and districts. Before sampling of the scales and sludges, these installations had already been operational for at least four years.

One of the installations from the South Holland region provided additional analysis information, henceforth referred to as company S. The geothermal water from the reservoir, geothermal brine, is monitored annually at production. Previous analysis (SGS Nederland, 2020) of the geothermal brine, collected and analysed in 2020, indicated 114500 mg L^{-1} of total dissolved solids (TDS), with the significant ion composition shown in Fig. 1. Strontium (400 mg L^{-1}) and Iron (32 mg L^{-1}) were also reported.

2.2. Sampling and initial preparation

During the annual maintenance and cleaning operation of one of the geothermal installations (company S), sludge was found and sampled in four different places in the installation after the drainage of the geothermal water (Fig. 2): the degasser (S1), the oil compartment of the degasser (S2), the pipelines before the filters (S3), and the residue in the filter itself (S4). The samples' mass varied accordingly: 346 g, 99 g, 426 g (without the water), and 613 g for S1, S2, S3, and S4, respectively. The sludge in the oil compartment resulted from a pressure loss during installation, causing the corrosion/scaling inhibitor to float on top of the brine and spill over into the oil compartment, which resulted in a more organic nature of sample S2.

Additionally, four scale samples, A, B, C, and D, were also provided from the decontamination of heat exchangers belonging to four different companies. The samples' mass varied respectively for samples A, B, C, and D: 18 g, 65 g, 30 g, and 50 g.

All the sludge samples were dried separately at 45 °C in an oven (Thermo Scientific, Heratherm OGH100) until a constant mass was achieved, which took about 15 days. The sludge found in the first compartment of the degasser (S1) had to be milled afterwards with a planetary ball mill (Retsch, PM 100) to improve the homogeneity of the sample as it hardened during the drying process. These sample preparation steps were executed before the characterisation. The scale samples were measured as provided by the companies.

2.3. Characterisation techniques

2.3.1. Energy dispersive X-ray fluorescence (EDXRF)

The EDXRF results provide insight into the samples' elemental composition for elements with an atomic number higher than sodium. This allows for self-attenuation calculation, which influences the detection efficiencies in gamma-ray spectrometry.

All the sludge and scale samples were analysed using a high-performance EDXRF spectrometer (XEPOS HE, Spectro Analytical Systems, Kleve, Germany). The 50 W/60 KV X-ray tube consists of a binary-alloy anode of cobalt (Co) and palladium (Pd), which allows sensitive analysis of elements from K to Mn, as the Co K-rays can more effectively irradiate these elements. The 60 kV provides extra power for analysing elements from Rh to Ce. The instrument is supplied with a Silicon Drift Detector (SDD). The analyser is configured to produce the best excitation conditions for a specified group of elements, using bandpass-filter

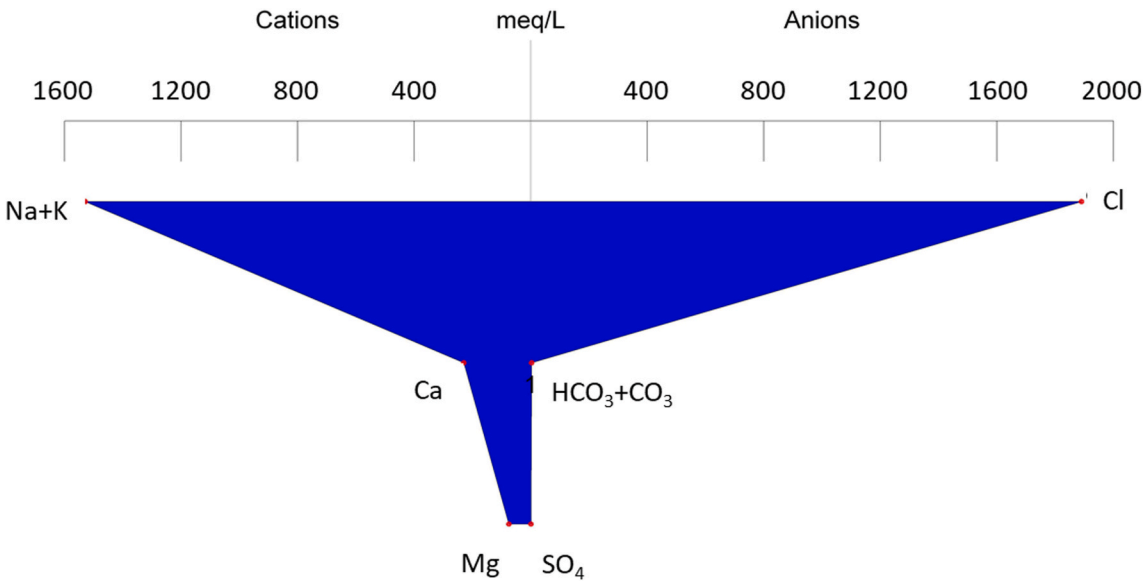

Fig. 1. Stiff diagram of major ion composition of the geothermal water.

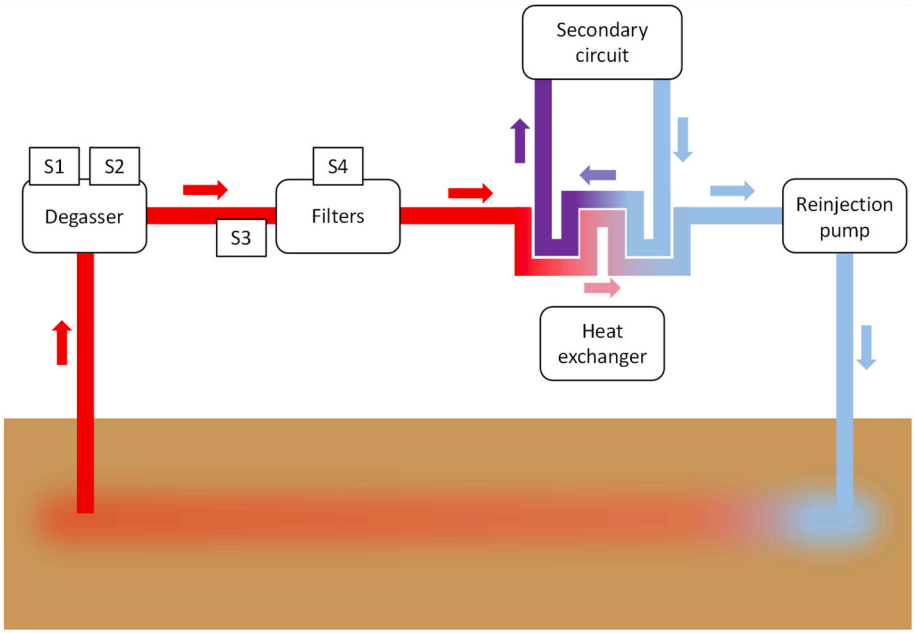

Fig. 2. Schematic overview of the geothermal installation of company S with sampling locations indicated.

excitation or combined polarised/direct excitation. This measurement was performed three times, allowing the calculation of the standard deviation of the measurements.

The dried and finely ground samples were analysed as loose powder. For analysis as a loose powder, an EDXRF sampling cup, provided with a 4 μm prolene foil (Chemplex®), was filled with the sample and subsequently placed in the autosampler of the EDXRF system. Quantification was performed using a TurboQuant II software package to screen unknown samples. Quality control is performed using certified reference materials.

2.3.2. *Gamma-ray spectrometry*

The sludge samples were measured using two High-Purity Germanium (HPGe) detectors, named Ge-T5 (Mirion Technologies (Canberra) model GC4020) and Ge-T6 (Mirion Technologies (Canberra) model BE2825P). Each lead castle consisted of 5 cm of lead, 5 cm of low-background lead (low ^{210}Pb content) and 2 mm of copper. Due to its thin micrometre-sized deadlayer, detector Ge-T6 was set to measure with high amplification in the low energy region to determine the ^{210}Pb activity using the 46.5 keV peak more precisely. The energy calibration of both detectors was done with sealed reference sources from Eckert & Ziegler Nuclitec GmbH. The relative efficiency of detector Ge-T5 is 40 %, and its energy resolution is 1.00 and 2.00 keV at full width at half maximum (FWHM) from 122 keV and 1332.5 keV, respectively. The relative efficiency of detector Ge-T6 is 18 %, and its energy resolution is 0.586 and 1.708 keV at FWHM, respectively, from 122 keV and 1332.5 keV. A single digital unit, Lynx®' recorded the spectra with 8192 channels. The scale samples were measured using the HPGe detector Ge-T6, with the Lynx® set to record the spectra with 32768 channels.

The efficiency transfer method was used to determine the gamma-rays' full energy peak efficiency (ε) for the radionuclides involved (Hult et al., 2021). This method relies on (i) measuring a reference source of

similar geometry as the samples of this study and (ii) correcting for differences between the reference sources and the samples using calculations with the Monte Carlo code EGSnrc (Hult et al., 2021), (Vidmar, 2005).

The samples were transferred to radon-tight Teflon containers, and the sample masses for samples A, B, C, D, S1, S2, S3, and S4 were 12 g, 36 g, 11 g, 37 g, 48 g, 96 g, 54 g, and 54 g, respectively. Since the massic activity of ^{226}Ra was calculated using the short-lived ^{222}Rn progenies ^{214}Pb and ^{214}Bi, secular equilibrium between ^{222}Rn and ^{226}Ra had to be ensured. This was achieved with a delay of at least 28 days between sample containment and measurement, corresponding to about 7 times the half-life of ^{222}Rn. Given its long-standing duration of at least 28 days, we can also assume that secular equilibrium was established between ^{234}Th and ^{238}U. When both ^{234}Th and ^{234m}Pa could be measured, the resulting massic activity for ^{238}U was the weighted mean value of the massic activities of ^{234}Th and ^{234m}Pa. A similar approach was used to quantify ^{228}Th based on several of its progeny.

The samples were measured for at least three days to ensure good counting statistics or until the significant gamma-ray peaks contained a net peak area of at least 10000 counts. An in-house developed software, GLysis (Lutter et al., 2018), was used for data analysis since it allows the calculation of the massic activity of the radionuclides based on selected gamma-ray lines. This offers the advantage of choosing easy-to-distinguish gamma-ray lines in the spectrum that have little to no interference. Table 1 reports the gamma-ray energies used. The massic activity of each radionuclide was determined as a weighted average based on the different gamma-ray lines. To subsequently determine the massic activity of a long-lived parent radionuclide of interest the weighted average massic activity of the progenies was taken, given secular equilibrium was established.

The combined standard uncertainty (k = 1) was calculated for each radionuclide, taking into account the uncertainties of each component in the equation used to convert count rate to massic activity. The major components were uncertainties linked to the FEP efficiency (generally 3 % but varying from 2 % to 10 % depending on the gamma-ray) and the calibration sources (1.5 %). In some cases, the emission probability (0.2 %–1.5 %) and count rate also made noticeable contributions. Monte Carlo simulations were performed to assess the contribution to the final uncertainty from parameters such as filling height, elemental composition, and bottom thickness of the sample container. Although certain uncertainties (like live time, mass, and decay corrections were negligible (in the order of a few tenths of a percent) they were anyhow included in the calculations. The uncertainties of the coincidence summing corrections were included in the Monte Carlo simulations, being an integral part of the efficiency transfer method and are included in the overall FEP efficiency uncertainty.

The gamma-ray spectrometry measurement was repeated for each sludge sample on average 340 days after sampling to monitor changes in the massic activity of the different radionuclides within their natural decay chain. For the scale samples, this was, on average, 53 days. This difference was due to practical time constraints. During this time, the samples remained encapsulated in the radon-tight containers. The exact time intervals for each sample, starting from the moment of sampling, can be found in Table 2. To ensure quality control during this process, the energy and efficiency calibration was verified by measuring Quality Assurance (QA) sources between each measurement. A certified volume source was used to check the Monte Carlo detector model.

2.3.3. Alpha-particle spectrometry

The eight samples were analysed with alpha-particle spectrometry to determine the massic activity of the thorium isotopes ^{232}Th, ^{230}Th, and ^{228}Th. Additionally, the scale samples (A-D) were also analysed to determine the massic activity of ^{210}Po.

The samples were destructed using microwave digestion. All the samples except sample S2 were dissolved using borate fusion and the Katanax X-300 instrument. In a Pt/Au crucible, approx. 0.1 g sample, 50/50 LiT/LiM and 0.1g LiBr were added. The ^{229}Th (~5 mBq) tracer was added, and the mixture was fused for 20 min. The liquid was poured in 40 mL 4 M HNO_3, thereafter, 1 mL of 100 g L^{-1} polyethylene glycol was added. After filtration of the resulting sample, a radiochemical separation of thorium isotopes was performed using TEVA® (Tetra Valent) resin. Due to the organic nature of S2, this was dissolved using HNO_3 and HCl and a microwave digestion system (CEM-SPD80). A mixture of 7 mL of 65 % HNO_3, 3 mL of 37 % HCl, and 3 mL of 50 % HBF_4 was used. A temperature up to 180 °C and a pressure of 400 PSI was applied of a complete dissolution. The resulting solution was evaporated to dryness and the residue was taken up in 10 mL of 4 M HNO_3. The chemical recovery (with 1s uncertainty) was 37 ± 4 %, 47 ± 5 %, and 19 ± 3 % for samples A, B, and C. Due to its high radioactivity levels, sample D was not analysed with alpha-particle spectrometry for the thorium isotopes. For samples S1, S2, S3, and S4 this was 107 ± 6.5 %, 100 ± 6.5 %, 65 ± 4.5 %, and 79 ± 5.5 %, respectively.

The TEVA® columns were conditioned with 4 M HNO_3, after which the samples were passed through. Thorium isotopes were eluted from the TEVA® column with 25 mL 9 M HCl. All the thorium isotope fractions were evaporated to dryness with electrodeposition on stainless steel discs for 4–5 h, according to the procedure described by Talvitie (1972) (Talvitie, 1972).

Table 2
Overview of exact time intervals in days between sampling and initiation of the measurements.

	A	B	C	D	S1	S2	S3	S4
1st gamma-ray measurement	536	469	359	295	196	192	174	156
2nd gamma-ray measurement	595	507	401	368	343	345	335	337
Alpha-particle spectrometry	590	498	405	380	439	439	439	439

Table 1
Overview of the radionuclides and their gamma-lines used for determining the massic activities with I_γ the emission probability.

	Nuclide of interest	Half-life	Measured nuclide	E_γ (keV) (I_γ)
^{238}U series	^{238}U	4.47E9 a	^{234}Th	63.3 (3.75 %). 92.4 (2.8 %). 92.8 (2.2 %)
			^{234m}Pa	766.4 (0.3 %). 1001 (0.8 %)
	^{226}Ra	1600 a	^{226}Ra	186.2 (3.6 %)
			^{214}Pb	242 (7.3 %). 295.2 (18.4 %). 351.9 (35.6 %)
			^{214}Bi	609.3 (45.5 %). 1120.3 (14.9 %). 1238.1 (5.8 %). 1764.5 (15.3 %)
	^{210}Pb	22.2 a	^{210}Pb	46.5 (4.3 %)
^{232}Th series	^{228}Ra	5.75 a	^{228}Ac	129.1 (2.5 %). 209.2 (4 %). 338.3 (11.4 %). 409.5 (2 %). 911.2 (26.2 %). 969 (15.9 %). 1459.1 (0.9 %)
	^{228}Th	1.9 a	^{224}Ra	241 (4.1 %)
			^{212}Pb	238.6 (43.6 %)
			^{212}Bi	727.3 (6.7 %). 1620.7 (1.5 %)
			^{208}Tl	583.2 (85 %). 860.5 (12.4 %). 2614.5 (99.8 %)
^{235}U series	^{235}U	7.04E8 a	^{235}U	143.8 (10.9 %). 163.4 (5.1 %). 185.7 (57 %). 205.3 (5 %)
Not applicable	^{40}K	1.25E9 a	^{40}K	1460.8 (10.6 %)

The determination of ^{210}Po in the scale samples was done by dissolving 0.05 g of the sample using microwave digestion system (CEM-SPD80). A small amount of sample was used due to the high radioactivity present in the sample. A known amount of ^{209}Po tracker was added to monitor the chemical recovery of the separation. Chemical recovery (with 1s uncertainty) of ^{209}Po was 63 ± 4.5 %, 51 ± 4 %, 45 ± 3.5 %, and 80 ± 7.5 for samples A, B, C, and D respectively. The spontaneous deposition of the polonium isotopes was performed using Ag disks for 6 h.

For the alpha-particle spectrometry measurements, PIPS® (Passivated Implanted Planar Silicon) semiconductor detectors of 600 mm^2 were used. The measurement time was 250000 s.

2.4. The Bateman equation

Calculation of the massic activity to the sampling date is trivial for ^{232}Th as it is the very long-lived parent of the decay chain, and it is not fed by any other radionuclide. However, due to the disequilibrium in the decay chain, ^{228}Ra and ^{228}Th massic activities at the sampling date cannot be calculated easily. Therefore, the application of the Bateman equations (Degering and Köhler, 2011), (Krane, 1988) are necessary as they can give the activity of progenies in a decay chain.

Bateman equations were solved to the third order for the decay chain of ^{232}Th – ^{228}Ra – ^{228}Th in MATLAB to recalculate the massic activity back to the sampling time for each sample individually (Krane, 1988). To evaluate the changes in the disruption of the equilibrium, the massic activity of ^{228}Ra and ^{228}Th was determined at two different times using gamma-ray spectrometry combined with alpha-particle spectrometry of the thorium isotopes. The result is the weighted mean of the calculations for each of the three measurements. The same principle was applied to the measurements of the scale samples to determine the massic activity of ^{210}Pb and ^{210}Po at the moment of sampling when the state of equilibrium could not be identified. Since the massic activity of ^{226}Ra in all samples was several orders of magnitude smaller than ^{210}Pb and ^{210}Po, its contribution during these calculations is negligible.

3. Results

The EDXRF results provide insight into the samples' composition and the amount of trace elements present (Table 3). LE is the collection of light elements that cannot be detected by XRF. It was assumed to be the remaining undetected mass fraction. They are replaced by oxygen in the material composition for the self-attenuation correction for the gamma-ray spectrometry measurements. Se and Hg concentrations were lower than the detection limit of 5 mg kg^{-1} for all samples and thus not included in the data.

The elemental composition of samples S1, S3, and S4 is similar and mainly consists of Silicon and Chlorine. The high level of Si indicates sandstone formation, identified as Slochteren sandstone (TNO-GDN and Formatie van Slochteren), from which the silica dissolves and precipitates in the sludge in the geothermal installation. The Chlorine is normal to be expected due to the contact with the brine. Sample S2 has a distinctly different composition (organic) and contains more heavy metals compared to the other sludges because of its origin in the oil compartment of the degasser. The main element in the scale samples A, B, and C is Iron, with a respective concentration of 22 wt%, 16 wt%, and 69 wt%. Sample D is different and mainly consists of Lead (48 wt%) and Sulphur (22 wt%).

In addition, some potentially hazardous elements, i.e. metals with high Z (atomic number), could be identified. Lead was found in significant amounts across all samples, up to 48 wt%, in sample D. Chromium was found in high amounts in all the samples, with varying

Table 3
Elemental composition determined using EDXRF (with the standard deviation). LE are light elements (mainly oxygen) not detected by EDXRF.

	Sample:	Scale				Sludge			
		A	B	C	D	S1	S2	S3	S4
Na	(g kg^{-1})	–	–	–	–	19 ± 0.1	24 ± 0.1	27 ± 0.1	29 ± 0.1
Mg	(g kg^{-1})	19 ± 0.1	9 ± 0.06	<1	<1	8 ± 0.06	24 ± 0.1	6 ± 0.02	5 ± 0.06
Al	(g kg^{-1})	8 ± 0.04	21 ± 0.1	<1	2 ± 0.2	83 ± 0.6	20 ± 0.1	66 ± 0.2	57 ± 0.2
Si	(g kg^{-1})	19 ± 0.02	65 ± 0.03	<1	14 ± 0.05	290 ± 2	49 ± 0.03	351 ± 0.2	350 ± 0.05
P	(g kg^{-1})	<1	1 ± 0.1	<1	2 ± 0.01	<1	6 ± 0.1	<1	<1
S	(g kg^{-1})	28 ± 0.4	6 ± 0.2	<5	223 ± 12	3 ± 0.2	6 ± 0.2	2 ± 0.1	2 ± 0.01
Cl	(g kg^{-1})	<1	<1	<1	<1	21 ± 0.3	<1	18 ± 0.6	17 ± 0.8
K	(g kg^{-1})	<1	2 ± 0.01	<1	<1	16 ± 0.01	11 ± 0.02	9 ± 0.03	8 ± 0.02
Ca	(g kg^{-1})	25 ± 0.05	43 ± 0.06	<5	23 ± 0.03	14 ± 0.02	10 ± 0.03	11 ± 0.03	12 ± 0.03
Ti	(g kg^{-1})	137 ± 0.4	15 ± 0.02	2 ± 0.01	<1	6 ± 0	4 ± 0.01	5 ± 0.01	5 ± 0
V	(mg kg^{-1})	<5	<5	<5	<5	220 ± 0.5	230 ± 0.1	316 ± 7	301 ± 10
Cr	(g kg^{-1})	3 ± 0.09	1 ± 0.2	14 ± 0.05	6 ± 0.04	2 ± 0.08	22 ± 0.5	2 ± 0.2	2 ± 0.02
Mn	(mg kg^{-1})	450 ± 13	2480 ± 44	12140 ± 26	620 ± 23	418 ± 11	5880 ± 225	427 ± 29	440 ± 9
Fe	(g kg^{-1})	221 ± 0.5	159 ± 0.04	694 ± 0.8	44 ± 0.04	42 ± 0.04	240 ± 0.5	39 ± 0.1	43 ± 0.1
Co	(mg kg^{-1})	<5	<5	<5	<5	31 ± 2	<5	22 ± 5	21 ± 0.4
Ni	(mg kg^{-1})	<5	250 ± 3	180 ± 5	44050 ± 211	128 ± 2	1040 ± 24	125 ± 7	124 ± 5
Cu	(g kg^{-1})	18 ± 0.5	2 ± 0.5	82 ± 0.5	7 ± 0.5	<1	3 ± 0.5	<1	<1
Zn	(mg kg^{-1})	7220 ± 164	22160 ± 451	890 ± 24	2920 ± 125	614 ± 16	630 ± 20	317 ± 29	374 ± 9
As	(mg kg^{-1})	280 ± 32	1510 ± 151	520 ± 35	2149 ± 34	37 ± 4	<5	44 ± 3	31 ± 7
Br	(mg kg^{-1})	<5	<5	<5	<5	226 ± 6	<5	210 ± 9	147 ± 35
Rb	(mg kg^{-1})	40 ± 0.8	<5	<5	<5	97 ± 0.7	90 ± 0.9	57 ± 0.8	58 ± 0.7
Sr	(mg kg^{-1})	1320 ± 79	4110 ± 249	780 ± 35	<5	517 ± 9	610 ± 27	495 ± 30	467 ± 38
Y	(mg kg^{-1})	90 ± 0.8	70 ± 0.6	<5	<5	25 ± 0.2	<5	17 ± 0.3	17 ± 0.2
Zr	(mg kg^{-1})	20 ± 6	1730 ± 137	180 ± 16	<5	167 ± 12	70 ± 5	182 ± 1	158 ± 14
Nb	(mg kg^{-1})	<5	10 ± 0.6	<5	1510 ± 12	16 ± 0.6	<5	17 ± 0.5	18 ± 0.2
Mo	(mg kg^{-1})	20 ± 0.4	80 ± 2	1110 ± 13	600 ± 6	19 ± 0.4	110 ± 24	24 ± 1	29 ± 2
Cd	(mg kg^{-1})	90 ± 0.4	150 ± 0.7	<5	840 ± 0.7	<5	<5	<5	<5
Sn	(mg kg^{-1})	180 ± 15	110 ± 12	270 ± 12	330 ± 15	5 ± 0.1	<5	6 ± 0.6	7 ± 0.6
Sb	(mg kg^{-1})	210 ± 11	110 ± 9	250 ± 12	690 ± 12	70.3 ± 0.3	90 ± 0.6	6 ± 0.3	6 ± 0.3
Ba	(mg kg^{-1})	7000 ± 438	45415 ± 1254	3470 ± 235	<5	331 ± 55	<5	402 ± 20	420 ± 12
Tl	(mg kg^{-1})	<5	<5	<5	<5	8 ± 0.4	<5	<5	7 ± 0
Pb	(g kg^{-1})	11 ± 0.6	31 ± 0.6	6 ± 0.6	477 ± 0.9	<1	3 ± 0.6	<1	<1
LE[a]	(g kg^{-1})	507	535	/	167	501	784	474	471

[a] Calculated by difference.

concentrations of up to one order of magnitude. Antimony was found in high concentrations in all four scale samples (A-D). It was also relatively high in sludge S2. Finally, Thallium was present only in S1 (8 mg kg^{-1}) and S4 (7 mg kg^{-1}). The concentration of rare earth elements (REE), such as Neodymium and Yttrium, is insufficient for exploring commercially viable retrieval options.

3.1. Gamma-ray spectrometry

The results of the first gamma-ray spectrometry measurement are shown in Table 4. Following the process line of the sludges (S1-S3-S4), an increasing massic activity of ^{226}Ra was observed, ranging from 52 Bq kg^{-1} (sample S1) to 86 Bq kg^{-1} (sample S4). At the same time, a decreasing massic activity of ^{210}Pb and ^{40}K are measured, respectively, ranging from 7600 Bq kg^{-1} to 760 Bq kg^{-1} and 570 Bq kg^{-1} to 250 Bq kg^{-1}. The deposition of the uranium isotopes ^{235}U and ^{238}U did not change significantly between the three sampling locations within one installation. In sample S2, only a detection limit could be determined for these radionuclides. Fig. 3 illustrates the difference in count rate in the spectra between samples S1 and S2, compared to the background on Ge-T5. The different activity levels of the samples is clearly reflected in the spectrum, which is also partially due to the difference in sample mass.

The variation of the radionuclide content in the scales between different samples of different installations is clearly demonstrated in Fig. 4, where the gamma-ray spectrum of scale samples B and D is shown. A peak at 803 keV could clearly be distinguished from the background in the spectrum of the scale sample D and was identified as the gamma-ray of ^{210}Po with a gamma-ray emission probability of 0.00123 %. A detection limit was set for the three samples A, B and C, while in sample D, a massic activity of 1970 kBq kg^{-1} was established. In addition to the low emission probability of the gamma-ray at 803 keV, the detection of ^{210}Po using gamma-ray spectrometry (which is not common) is hampered by the fact that there is a peak in the background at exactly the same energy, as it is the same transition in the nucleus of ^{206}Pb. The background peak originates from neutron interaction with the lead shield and is affected by changes in the cosmic ray flux.

Uranium isotopes could not be detected in scale samples A, C, and D. The amount found in sample B was similar to that in the sludge samples. The scale samples contain lower ^{40}K and higher amounts of ^{226}Ra and ^{210}Pb than the sludge samples.

Furthermore, as seen in Table 4, all eight samples had, at the time of starting the first measurement, higher ^{228}Th activity than ^{228}Ra activity. For seven of the samples, the ratio ranged from 1.41 (sample B) to 97 (sample S2). Only for scale sample C is ^{228}Th/^{228}Ra ratio close to one, which could give the impression that there is secular equilibrium with ^{232}Th, which requires a ratio of 1.0. However, since this ratio can be by coincidence 1, it is not possible to say whether this is the case based on one measurement.

The difference in the ^{228}Th/^{228}Ra ratio between the sludge and scale samples highlights the different properties of the scale and sludge and the enrichment of ^{228}Th. This emphasises the diverse properties and deposition mechanisms of these elements. Thorium is more likely to adhere to the corrosion and scaling inhibitor or deposits in the heat exchanger due to fluctuating temperature conditions, whereas ^{228}Ra remains more soluble in the thermal water under these circumstances.

A disruption in the ^{210}Pb-^{210}Po equilibrium is also noted in sample D, which has a ^{210}Po/^{210}Pb ratio of 14. It was not possible to assert this with certainty regarding the other scale samples A, B, and C.

Compared to the first measurement, the second gamma-ray spectrometry measurement (Table 5) shows a slight decrease in the ^{228}Th massic activity for samples D, S1, S2, S3, and S4 but not for ^{228}Ra. For sample D, the ^{228}Ra was below the detection limit. The ^{228}Th/^{228}Ra ratio decreases by 5 %, 7 %, 14 %, 0.8 %, and 6 % for the five samples, respectively. In sample C, the ^{228}Th/^{228}Ra ratio remained close to one, and the individual massic activities stayed consistent within the uncertainty, again implying secular equilibrium with ^{232}Th. For the other radionuclides, no clear trend or change could be discerned.

The equilibrium status depends on the initial massic activity of the different radionuclides. Since the half-lives of ^{228}Ra (5.75 a) and ^{228}Th (1.91 a) are relatively short compared to the half-life of ^{232}Th (1.40E10 a), changes in the ratio of the massic activity of ^{228}Ra and ^{228}Th are noticeable after a few months. The repeated gamma-ray spectrometry measurements allow monitoring changes in the massic activity before reaching secular equilibrium with ^{232}Th. The massic activity of ^{228}Th decreased more than the massic activity of ^{228}Ra in all samples. A similar description applies to the ^{210}Pb-^{210}Po equilibrium. Although the half-life of ^{210}Po is only 138.4 days, there is no significant change in the massic activity in sample D observed after 73 days. However, the uncertainty on the first measurement result is too high to clearly observe the expected decrease in activity.

3.2. Alpha-particle spectrometry

Alpha-particle spectrometry analysis (Table 6) showed an elevated massic activity of ^{228}Th compared to the relatively low massic activity of ^{232}Th for all the samples. Additionally, for all the sludge samples (S1-S4), ^{228}Th massic activity measured with alpha-particle spectrometry was lower for all four samples than the gamma-ray spectrometry measurements, also after decay correction. Within the uncertainty, the ratio of the gamma-ray and alpha-particle spectrometry measurements of sludge samples overlap with 1.0, except for sample S2, where the ratio is close to a factor of 1.7. For this sample (S2), a hypothesis for the higher ratio can be a possible interference of ^{210}Po (5.3 MeV) in ^{228}Th (5.34 MeV of 27 % intensity) alpha peak. If the sample contains high amounts of ^{210}Po, it is possible that during the radiochemical purification of the Th isotopes, traces of ^{210}Po are eluted together resulting in an overestimation of the ^{228}Th massic activity. For the scale samples A, B, and C, the ratio was 1.11 ± 0.31, 2.03 ± 0.32 and 0.55 ± 0.40, respectively. The thorium isotopes in sample D were not measured because the gamma-ray spectrometry measurements indicated that their levels were

Table 4
Massic activity of detected radionuclides in Bq kg^{-1} from the first gamma-ray spectrometry measurements given at the start of the measurement. The combined standard uncertainty (k = 1) is given between brackets. The detection limit has a confidence level of 90 %.

	Scale				Sludge			
	A	B	C	D	S1	S2	S3	S4
^{238}U	–	9.6E+01 (21)	–	–	5.3E+01 (5)	<4.0E+01	6.1E+01 (5)	5.6E+01 (5)
^{226}Ra	7.16E+02 (21)	3.28E+03 (10)	2.51E+02 (8)	3.6E00 (11)	5.20E+01 (17)	7.8E+01 (3)	8.3E+01 (3)	8.6E+01 (3)
^{210}Pb	1.68E+05 (16)	1.72E+05 (17)	2.5E+03 (3)	1.41E+05 (14)	7.6E+03 (8)	5.2E+03 (5)	7.9E+02 (8)	7.6E+02 (8)
^{210}Po	<2.1E+05	<1.5E+05	<1.3E+05	2.0E+06 (8)	–	–	–	–
^{228}Ra	3.93E+02 (16)	5.45E+02 (22)	1.18E+02 (5)	3.2E00 (6)	5.9E+01 (4)	1.03E+02 (9)	5.9E+01 (4)	6.7E+01 (4)
^{228}Th	1.75E+03 (7)	7.7E+02 (3)	1.17E+02 (5)	1.03E+01 (14)	1.08E+02 (4)	1.00E+04 (4)	8.5E+01 (3)	1.28E+02 (5)
^{235}U	–	1.10E+01 (20)	–	–	2.1E+00 (3)	<1.8E00	2.9E+00 (3)	2.5E+00 (4)
^{40}K	1.8E+01 (15)	<1.8E+02	–	<8.1E00	5.7E+02 (4)	2.00E+02 (13)	2.68 + 02 (16)	2.53E+02 (16)
^{228}Th/^{228}Ra	4.5 ± 0.3	1.41 ± 0.08	0.99 ± 0.06	3.2 ± 0.8	1.83 ± 0.14	97 ± 9	1.43 ± 0.11	1.90 ± 0.14

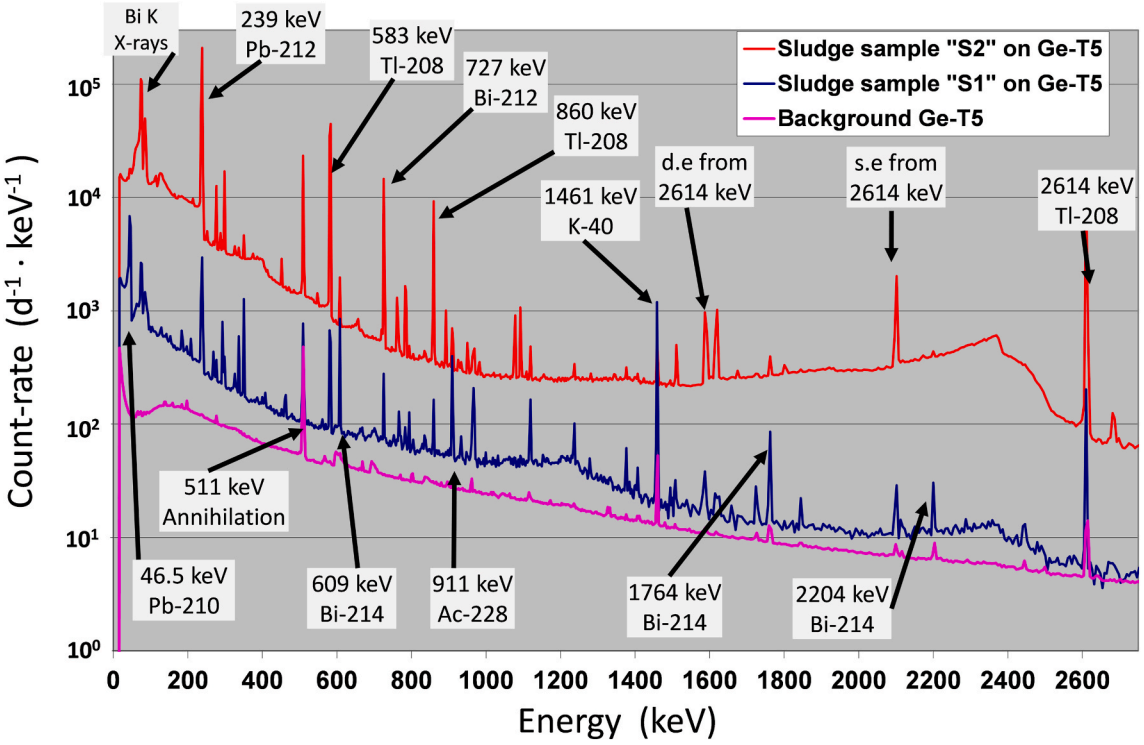

Fig. 3. Gamma-ray spectra of samples S1 (48 g) and S2 (96 g) compared to the background of detector Ge-T5. The single and double escape peaks are denoted s.e. and d.e., respectively.

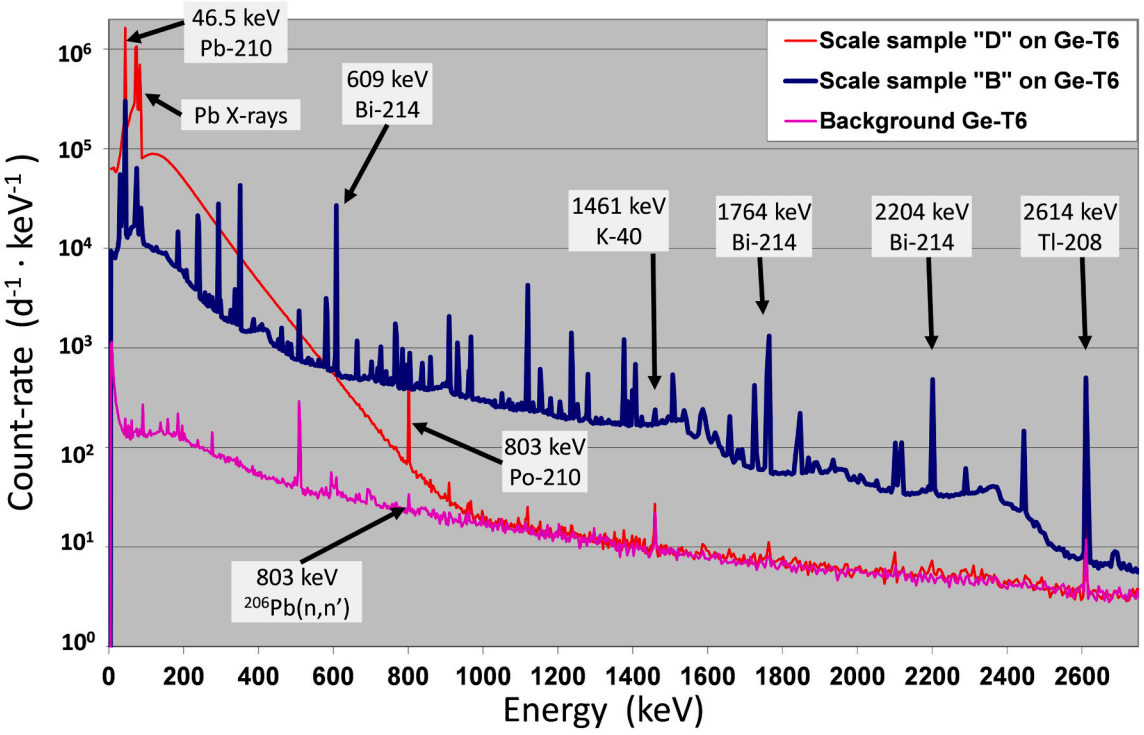

Fig. 4. Gamma-ray spectra of samples B and D compared to the background, measured on Ge-T6.

too low to obtain meaningful results.

The ^{210}Po measurements of samples A, B, and C aligned with the detection limits previously established with gamma-ray spectrometry. On the other hand, the massic activity measured in sample D was a factor 2 higher than initially measured by gamma-ray spectrometry. As it can be seen from Table 6, ^{210}Po has the highest massic activity from all the radionuclides identified in these samples. Given the high radiotoxicity, safety measures must be ensured during the cleaning and decontamination of the heat exchangers.

Table 5
Massic activity of detected radionuclides in Bq kg^{-1} from the second gamma-ray spectrometry measurements given at the start of the measurement. The combined standard uncertainty (k = 1) is given between brackets. The detection limit has a confidence level of 90 %.

	Scale				Sludge			
	A	B	C	D	S1	S2	S3	S4
^{238}U	–	–	–	–	4.2E+01 (4)	<2.9E+01	6.4E+01 (5)	5.3E+01 (6)
^{226}Ra	7.07E+02 (21)	3.32E+03 (10)	2.49E+02 (8)	3.2E00 (7)	5.30E+01 (18)	9.9E+01 (4)	8.3E+01 (3)	8.7E+01 (3)
^{210}Pb	1.67E+05 (16)	1.7E+05 (2)	2.25E+03 (23)	1.4E+05 (1)	7.5E+03 (8)	5.5E+03 (6)	7.7E+02 (8)	7.5E+02 (8)
^{210}Po	<2.0E+05	1.7E+05 (3)	<1.0E05	2.0E+06 (1)	–	–	–	–
^{228}Ra	3.78E+02 (15)	5.30E+02 (21)	1.10E+02 (5)	<3.5E00	6.0E+01 (4)	1.13E+02 (11)	5.8E+01 (4)	6.6E+01 (4)
^{228}Th	1.67E+03 (7)	7.8E+02 (3)	1.16E+02 (5)	8.0E00 (9)	1.02E+02 (4)	8.8E+03 (4)	8.2E+01 (3)	1.18E+02 (5)
^{235}U	<4.1E00	–	–	–	1.9E+00 (3)	<1.3E00	2.5E+00 (3)	2.5E+00 (3)
^{40}K	–	4.1E+01 (5)	<2.1E+01	<1.0E+01	5.7E+02 (4)	1.83E+02 (13)	2.60 + 02 (16)	2.52E+02 (16)
^{228}Th/^{228}Ra	4.4 ± 0.3	1.46 ± 0.08	1.05 ± 0.06	<2.3	1.70 ± 0.13	84 ± 7	1.38 ± 0.10	1.79 ± 0.13

Table 6
Massic activity of analysed radionuclides in Bq kg^{-1} from the alpha-particle spectrometry measurements given at the start of the measurement. The combined standard uncertainty (k = 1) is given between brackets. The detection limit has a confidence level of 90 %.

	Scale				Sludge			
	A	B	C	D	S1	S2	S3	S4
^{232}Th	<4.0E+01	<4.0E+01	<9.0E+01	–	3.0E+01 (3)	1.00E+01 (20)	2.5E+01 (3)	2.5E+01 (3)
^{230}Th	<5.0E+01	<4.0E+01	<1.0E+02	–	3.6E+01 (3)	1.5E+01 (3)	5.5E+01 (5)	5.0E+01 (4)
^{228}Th	1.50E+03 (20)	3.8E+02 (6)	2.1E+02 (6)	–	7.6E+01 (6)	4.6E+03 (6)	7.8E+01 (7)	9.1E+01 (7)
^{210}Po	2.10E+05 (15)	1.70E+05 (15)	2.0E+03 (7)	4.2E+06 (4)	–	–	–	–

4. Massic activity at the sampling date

Using the results from both gamma-ray and alpha-particle spectrometry measurements for the available radionuclides, the Bateman equations were used to calculate the massic activity at the sampling date for each sample individually (Table 7). As an example, Fig. 5 shows the massic activities for ^{232}Th, ^{228}Ra, and ^{228}Th as a function of time for sample S4. Due to disruption of the equilibrium, the virtual half-life of ^{228}Th immediately after sampling was derived from the fitted curve and found to be 3.89 a. It differs from those of ^{228}Ra and ^{232}Th, yet is longer than the ^{228}Th half-life. As equilibrium progressively approaches over time, this virtual half-life of ^{228}Th will first go towards the ^{228}Ra half-life and later towards that of ^{232}Th.

Since the ^{228}Th/^{228}Ra ratio in sample C is 1 within the uncertainty for both with the gamma-ray spectrometry measurements, secular equilibrium between these two radionuclides was assumed. However, alpha-particle spectrometry showed a significantly lower ^{232}Th massic activity than the massic activities of ^{228}Ra and ^{228}Th, indicating that there is no secular equilibrium between ^{232}Th and its progenies ^{228}Ra and ^{228}Th. On the other hand, the ^{228}Th massic activity using gamma-ray spectrometry does not align with the one obtained with alpha-particle spectrometry. With the absence or very low activity of ^{232}Th, there is also a possibility for transient equilibrium to be established. In this case, the ^{228}Th/^{228}Ra activity ratio would need to be 1.5. This discrepancy may be attributed to sample inhomogeneity and the small

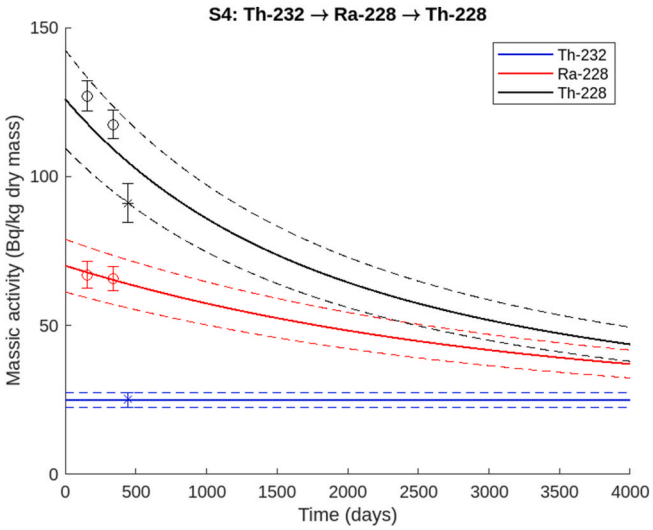

Fig. 5. Visualisation of the equilibrium by solving the Bateman equations using the measurement data for the radionuclides ^{232}Th, ^{228}Ra, and ^{228}Th of sample S4 (the weighted uncertainty represented as a dotted line), according to gamma-ray (o) and alpha-particle spectrometry (*) results, including its combined standard uncertainty. Time zero is at the sampling date.

Table 7
Calculated massic activity in Bq kg^{-1} at sampling date for the different radionuclides. The combined standard uncertainty (k = 1) is given between brackets.

	Scale				Sludge			
	A	B	C	D	S1	S2	S3	S4
^{238}U	–	–	–	–	4.8E+01 (3)	<4.0E+01	6.2E+01 (3)	5.5E+01 (4)
^{226}Ra	7.1E+02 (2)	3.3E+03 (10)	2.5E+02 (1)	3.4E00 (6)	5.24E+01 (12)	9.04E+01 (25)	8.3E+01 (18)	8.63E+01 (19)
^{210}Pb	1.8E+05 (2)	1.8E+05 (2)	2.5E+03 (2)	1.4E+05 (1)	7.7E+03 (5)	5.4E+03 (4)	8.0 E+02 (6)	7.7E+02 (6)
^{210}Po	9.4E+05 (12)	1.8E+05 (3)	2.1E+03 (8)	8.3E+06 (10)	–	–	–	–
^{232}Th	<4.0E+01	<4.0E+01	<9.0E+01	–	3.0E+01 (3)	<1.0E+01	2.5E+01 (3)	2.5E+01 (3)
^{228}Ra	4.6E+02 (2)	6.3E+02 (3)	1.1E+02 (1)	<5.0E00	6.2E+01 (5)	1.12E+02 (17)	6.1E+01 (5)	7.0E+01 (6)
^{228}Th	6.7E+03 (1)	8.7E+02 (3)	1.2E+02 (1)	1.7E+01 (9)	1.17E+02 (6)	1.10E+04 (10)	9.0E+01 (5)	1.29E+02 (7)
^{235}U	–	–	–	–	2.0E+00 (2)	<1.8E00	2.74E+00 (21)	2.50E+00 (23)
^{40}K	1.8E+01 (15)	4.1E+01 (5)	<2.1E+01	<1.0E+01	5.7E+02 (3)	1.93E+02 (9)	2.64E+02 (12)	2.52E+02 (11)

sample intake for alpha-particle spectrometry.

Regarding ^{210}Pb-^{210}Po equilibrium in samples B and C, the individual measurements indicate that transient equilibrium between these two elements has been established. When using the Bateman equations to correct for the decay of ^{210}Pb and ^{210}Po, the decay of the longer-lived parent radionuclide, ^{226}Ra, was not considered in the calculations. Its massic activity is several orders of magnitude lower than that of ^{210}Pb, rendering its effect negligible.

5. Discussion

5.1. Toxic elements

The elemental composition of the samples is derived from the EDXRF measurements. There were several substances classified as dangerous by the Council of the European Union (Council of the European Union, 2000), such as Lead, Arsenic, Cadmium, Thallium and Chromium. Each element is allocated several Hazard statement Code(s); Arsenic: H331, H301, H410; Cadmium: H332, H312, H302, H400, H410; Lead: H360-DF, H332, H302, H373**, H400, H410; Thallium: H330, H300, H373**, H413 [(Council of the European Union, 2008a), Table 3.1]. For the same codes, the sum of the content cannot exceed the levels mentioned in Annex III of (Council of the European Union, 2008b). For example, the level of acute toxicity 1, 2, or 3 is determined by the sum of the concentrations of the elements with labels H300, H310, H330, H301, H311, and H331, which is both Thallium and Arsenic. The cut-off value acute toxicity 1, 2, or 3 following oral or dermal administration or inhalation exposure is 0.1 %, which is exceeded in sample B (0.15 %) and D (0.21 %).

The impact of these elements on human health depends not only on the concentration but also on the exposure route, the duration and the frequency of the exposure. Appropriate personal protective equipment (PPE) is imposed to avoid direct contact during maintenance operations. Furthermore, regular monitoring and maintenance schedules are essential to ensure that exposure remains within safe limits. In addition, it is advised to raise awareness through training programs for workers to enhance the proper use of PPE and adherence to safety protocols, further minimising health risks associated with prolonged exposure.

5.2. Radiometric characterisation

The study demonstrates that gamma-ray spectrometry is a valuable technique for the radiometric characterisation of samples from geothermal installations. It allows the analysis of multiple radionuclides in a single test with limited preparation steps compared to radiochemistry. However, due to the inhomogeneous nature of many NORMs, adequate sample preparation is necessary to acquire reliable results, as a high degree of sample homogeneity is essential for good results. Still, due to the relatively large sample intake, gamma-ray spectrometry is better than methods with a small sample intake to cope with a limited amount of inhomogeneities in the sample. Therefore, for accurate analysis, it is necessary to care for sample drying (and measuring the moisture content), milling, and mixing, which can be complicated to perform when dealing with highly active samples.

The disruption in the equilibrium of the ^{232}Th decay chain comes from separation during both the geothermal reservoir flow system and the industrial process in a geothermal installation. The world average concentration of ^{232}Th within the Earth's crust is 40 Bq kg^{-1} (Publication Office of the European Union, 2000). In the region of the geothermal installations, the estimated topsoil concentration of uranium is 7–9.3 mg kg^{-1} (Cinelli et al., 2019), resulting in an estimated massic activity of 28–38 Bq kg^{-1}. The radionuclide ^{232}Th is relatively immobile and tends to remain within the geothermal formation. Because of its low solubility, only small amounts of Thorium are brought to the surface during geothermal water extraction. Due to the reduced conditions, the ^{232}Th remaining in the geothermal formation decays to ^{228}Ra, which is highly soluble in geothermal water. The presence of Calcium and Strontium in the analysed geothermal water also indicates the likelihood of Radium being present, owing to their similar chemical properties. Subsequently, ^{228}Ra decays into ^{228}Th, which is again immobile and becomes insoluble in the process, easily attaching to impurities and precipitating in the geothermal installation, resulting in an elemental separation upon deposition.

Compared to the other sludge samples, sample S2 has a higher massic activity of ^{228}Ra and ^{228}Th and lower massic activity of ^{40}K, ^{238}U, and ^{235}U. The pressure loss and the corrosion/scaling inhibitor floating on top of the brine, spilling into the oil compartment, led to additional separation of thorium from the geothermal water. As sample S2 shows, not only environmental conditions but also unexpected operational conditions in the geothermal plant can result in massic activities that are different from the expected and consequently highlight the need for adequate monitoring measures.

All the samples exhibited a significantly lower massic activity of ^{226}Ra compared to ^{210}Pb. Additionally, a disruption in the equilibrium between ^{210}Pb and ^{210}Po was found in samples A and D. This suggests that the installations' varying temperature and pressure conditions are more favourable for the precipitation of Lead and Polonium than Radium, leading to an accumulation of Pb and even more Polonium in the scales and sludges. Often, ^{210}Po is assumed to be in equilibrium with ^{210}Pb. The high massic activities of ^{210}Po may remain undetected during routine monitoring since the probability of gamma-ray emission for ^{210}Po is only 0.00123 % and, therefore, difficult to detect using gamma-ray spectrometry. This can lead to a serious underestimation of the hazard when handling these materials. Furthermore, a high lead content or the presence of other high-z elements in the sample makes it very difficult to accurately assess the ^{210}Pb activity using gamma-ray spectrometry due to the low energy of its 46.5 keV gamma-ray. This can lead to both overestimation and underestimation of ^{210}Pb in a sample.

The massic activities of ^{226}Ra were relatively similar to those of ^{228}Ra in all the samples. This indicates, as expected, that the two radium isotopes are equally soluble in the water (Eggeling et al., 2013), as opposed to their parent nuclides, ^{238}U and ^{232}Th. However, the massic activity of the radium isotopes in the scale samples was at least one order of magnitude higher than that found in the sludge samples, except for sample D, where relatively low concentrations were found for these radionuclides. These relatively low activities also result in modest Radon concentrations. The inhalation of radon should not be ignored; however, a balance between rigorous safety measures and practicality is essential. To conduct a more comprehensive radon risk assessment, the radon concentration should be monitored during the filter exchange and maintenance/decontamination work, as standard practice indicates that these operations should be carried out in well-ventilated conditions while wearing PPE to protect against all radionuclides and hazardous elements.

Within the uranium decay chain, the ^{210}Pb massic activity is high compared to its parent nuclides ^{238}U and ^{226}Ra. The activity is fed through the decay of ^{226}Ra carried along in the geothermal brine and released from the geothermal formation. The progeny radionuclides between ^{226}Ra and ^{210}Pb are generally too short-lived to consider independent behaviour during the industrial process, although ^{222}Rn (3.8 days half-life) can complicate the situation as an inert gas. The massic activity of ^{210}Pb in the sludges is lower in the degasser compared to the region of the filters. The circumstances in the degasser and the heat exchangers are favourable for lead to co-precipitate with Sulphur or Phosphorus. These are insoluble and immobile compounds of lead in the environment (Lenntech). Lead first precipitates partially at the bottom of the degasser, while the remaining lead is captured in the filters or precipitates in the heat exchangers. The lead content measured with XRF is consequently also an indication of the massic activity of ^{210}Pb in the samples.

5.3. Regulation

The massic activity of ^{40}K is higher in the sludge samples compared to the scale samples, ranging from 200 to 570 Bq kg^{-1}. This radionuclide is already widely present in the environment, exhibiting an activity concentration in the sludge samples one order of magnitude higher than ^{232}Th and ^{238}U in the soil (UNSCEAR, 2000). The massic activity found in the scale samples is of the same order of magnitude as that found in the soil. Therefore, this radionuclide is not further discussed in detail in this study.

The Dutch regulation (*Besluit Basisveiligheidsnormen Stralingsbescherming*, 2024; Art 3.17) (Rijksoverheid, 2024) sets requirements for operations with radioactive substances and applies nuclide-specific limits. The massic activity levels of the different radionuclides (^{226}Ra+, ^{210}Pb+, ^{228}Ra+ and ^{228}Th+) are noted, where "+" signifies that the stated parent nuclide is in secular equilibrium with its progenies. The regulation distinguishes three categories. When the massic activity of the radionuclides remains below 1000 Bq kg^{-1}, only a notification has to be made to the authorities. A registration must be submitted when the massic activity is between 1000 Bq kg^{-1} and 10000 Bq kg^{-1}. In this situation, the residues are classified and need to be disposed of as hazardous waste. Above 10000 Bq kg^{-1}, the operator needs to apply for a permit, and these residues are classified and disposed of as NORM waste. When considering samples S3 and S4, a notification is sufficient. The high massic activities of ^{210}Pb in samples S1 and S2, 7550 Bq kg^{-1} and 5180 Bq kg^{-1}, respectively, and of ^{228}Th in sample S2, 9810 Bq kg^{-1}, ensure that the installation is subject to registration requirements according to the Dutch legislation (Rijksoverheid, 2024). However, the massic activity of ^{228}Th, calculated for the sampling date, in sample S2 is slightly higher than the limits for the registration requirements. Taking into account the rare nature of this sample and the uncertainty of the measurement, it should be sufficient to store this material on a short-term basis before disposal.

The activities measured of ^{210}Pb in the scale samples A, B, and D are higher than the 10000 Bq kg^{-1} imposed by the Dutch regulation (*Besluit Basisveiligheidsnormen Stralingsbescherming*, 2024; Art 3.17) (Rijksoverheid, 2024). They are, therefore, also considered NORM waste. Since the highest massic activity of sample C, during the decontamination, is between 1000 Bq kg^{-1} and 10000 Bq kg^{-1} for ^{210}Pb, this residue falls in the second category and needs to be handled as hazardous waste.

The exempt release conditions for wet sludges and materials in the geothermal industry in the Netherlands are 5000 Bq kg^{-1} for ^{226}Ra+, 100000 Bq kg^{-1} for ^{210}Pb+ and ^{40}K, 10000 Bq kg^{-1} for ^{228}Ra+, 1000 Bq kg^{-1} for ^{228}Th (van Bochove, 2023). As a result, samples S1, S3, and S4 are considered exempted waste (even after removing excess water) when disposed of shortly after decontamination, which, in this context, refers to the sampling date. This assessment also provides information used for radiation protection purposes. Sample S2 is considered NORM according to these regulations as the massic activity of ^{228}Th is higher than 1000 Bq kg^{-1}. Because of the relatively fast decay of ^{228}Th, with additional sampling and measurements, short-term storage on site and annual monitoring of the massic activity of ^{228}Th in the material of sample S2 is recommended. The material can remain in short-term storage until it has sufficiently decayed and can be handled as exempted material.

Since the half-life of ^{228}Th is influenced by the decay of its parent nuclides ^{232}Th and ^{228}Ra, measuring and following up the changes in the massic activity of ^{228}Th is advised. The relatively long half-life of ^{210}Pb (22 a) makes it difficult to arrange for on-site storage, as the long-term operation of such a small-scale geothermal facility has been difficult to predict for several decades.

5.4. Radiometric method SOP recommendation

Using a single technique, such as gamma-ray spectrometry, provides an excellent way to obtain accurate information about the temporal evolution of the sample's activities when performing successive measurements several months apart. When it comes to ^{210}Po, gamma-ray spectrometry may not be sufficient to characterise residues in the geothermal industry, as it is not necessarily in equilibrium with ^{210}Pb. However, an important conclusion of this work is that gamma-ray spectrometry practitioners should look for the weak 803 keV gamma line from ^{210}Po to identify very high levels of ^{210}Po. This practice is not straightforward, as the 803 keV line is standard in the background of many HPGe-detector systems as it is produced by neutron interaction with the detector's lead shield and varies with changes in cosmic flux. This highlights the fact that an important aspect to consider is that a specific radiometric technique has a bias or systematic uncertainty that influences the accuracy of the massic activity when operational or environmental conditions and sample characteristics change, such as variations in cosmic ray flux or elemental composition.

Given prior knowledge of the radionuclide content in the scale samples, a decision was made to minimise sample preparation steps. To reduce the risk of contamination and safeguard radiation protection, no milling, mixing, or sieving was performed for these samples, acknowledging that a potential inhomogeneity may still be present. This inhomogeneity is reflected in the discrepancy between alpha-particle and gamma-ray spectrometry results for the ^{228}Th and ^{210}Po massic activities. The sample intake for gamma-ray spectrometry measurements (typically in the order of 100 g) is significantly higher than the 0.1 g used for alpha-particle measurements. Consequently, sample inhomogeneity has a greater impact on alpha-particle spectrometry results. To obtain a less biased value or at least a better understanding of the uncertainties of the absolute values of the massic activities, it is advisable to combine alpha-particle and gamma-ray spectrometry to detect and quantify the present radionuclides in the initial phase. While this may not be mandatory as a standard operating procedure at a geothermal plant, it could be beneficial to carry out extended measurement campaigns with both techniques at less regular intervals, particularly at the beginning of plant operation, such as for benchmarking and quality control.

6. Conclusion and outlook

Four sludge and four scale samples were collected during the maintenance and decontamination of geothermal installations in the Netherlands. Sludge samples S1 (degasser), S3 (pipeline before filter), and S4 (filter) mainly consist of Silicon and Chlorine. On the other hand, sample S2 from the oil compartment of the degasser had a completely different elemental composition, dominated by Iron and chromium. The scale samples A, B, and C mainly consisted of Iron. In contrast, the main elemental composition of sample D consisted of Lead and Sulphur. Several hazardous elements, such as Lead, Chromium, Arsenic, and Thallium, are present in varying concentrations, potentially posing health risks upon contact. Wearing appropriate personal protective equipment (PPE) remains crucial to minimise these risks. Gamma-ray and alpha-particle spectrometry measurements revealed disequilibria in the decay chains of ^{232}Th and ^{238}U. This resulted in ^{228}Th having the highest massic activities in the ^{232}Th decay chain and an enrichment of ^{210}Po relative to the massic activity of ^{210}Pb and ^{210}Pb relative to the massic activity of ^{226}Ra. The Bateman equations were used to calculate the massic activity at the sampling date for ^{228}Ra and ^{228}Th. The massic activity of ^{228}Th at the sampling date ranged from 93 Bq kg^{-1} (S3) to 12.3 kBq kg^{-1} (S2). The ^{226}Ra and ^{228}Ra massic activities were similar and lower than ^{228}Th activities. Significant massic activities for ^{210}Pb were measured with gamma-ray spectrometry in the scale samples, up to 180 kBq kg^{-1} (A and B). The highest activities were detected for ^{210}Po also in the scale samples, ranging from 2.1 kBq kg^{-1} (C) to 8.3 MBq kg^{-1} (D).

Gamma-ray spectrometry is a highly valuable analytical technique for obtaining accurate information on the evolution of radionuclide activities in geothermal samples. For a comprehensive characterisation

of the different radionuclides and to minimise bias and systematic uncertainty, it is recommended to combine alpha-particle and gamma-ray spectrometry. As complications may arise from sample inhomogeneity, gamma-ray spectrometry offers the advantage of accommodating a relatively large sample mass, thereby reducing the uncertainty associated with inhomogeneous materials.

In conclusion, in addition to this being the first time this type of study has been reported from installations in the Netherlands, it can be inferred that radiometric measurements of samples from geothermal installations encounter numerous challenges. Inhomogeneous samples with decay chains in disequilibrium and high sample composition variability can complicate correct interpretation for assessing radiation protection measures and waste treatment. An important aspect is to ensure that operators and radioanalytical laboratories are aware of the potential problems in interpreting analytical results and take appropriate measures correctly.

CRediT authorship contribution statement

Linde Pollet: Writing – review & editing, Writing – original draft, Visualization, Methodology, Formal analysis, Data curation, Conceptualization. **Mikael Hult:** Writing – review & editing, Writing – original draft, Validation, Supervision, Methodology, Data curation, Conceptualization. **Mirela Vasile:** Writing – review & editing, Writing – original draft, Supervision, Formal analysis. **Gerd Marissens:** Writing – review & editing, Supervision, Data curation. **Heiko Stroh:** Writing – review & editing, Supervision, Data curation. **Sonja Schreurs:** Writing – review & editing, Supervision, Data curation. **Wouter Schroeyers:** Writing – review & editing, Writing – original draft, Supervision, Methodology, Funding acquisition, Conceptualization.

Declaration of competing interest

The authors declare that they have no known competing financial interests or personal relationships that could have appeared to influence the work reported in this paper.

Acknowledgement

We are greatly indebted to Prof Anita Erőss (ELTE, Budapest) for insightful comments on the manuscript. This project has received funding from the Euratom research and training programme 2019–2020 under grant agreement No 900009 (RadoNorm) and runs under the Collaborative Doctoral Partnership between JRC and UHasselt, agreement number 35342.

Data availability

No data was used for the research described in the article.

References

Bertani, R., 2016. Geothermal power generation in the world 2010–2014 update report. Geothermics 60, 31–43. https://doi.org/10.1016/j.geothermics.2015.11.003.

Cinelli, G., De Cort, M., Tollefsen, T., 2019. European Atlas of Natural Radiation. Publication Office of the European Union, Luxembourg.

Council of the European Union, 2000. 2000/532/EC: Commission Decision of 3 May 2000 replacing Decision 94/3/EC establishing a list of wastes pursuant to Article 1 (a) of Council Directive 75/442/EEC on waste and Council Decision 94/904/EC establishing a list of hazardous waste pursuant to art. Off. J. Eur. Union [Online]. https://eur-lex.europa.eu/eli/dec/2000/532/oj/eng. (Accessed 17 October 2025).

Council of the European Union, 2008a. REGULATION (EC) no 1272/2008 OF THE EUROPEAN Pon classification, labelling and packaging of substances and mixtures, amending and repealing Directives 67/548/EEC and 1999/45/EC, and amending Regulation (EC) no 1907/2006ARLIAMENT AND OF THE COUNCIL. Off. J. Eur. Union.

Council of the European Union, 2008b. Directive 2008/98/EC on waste and repealing certain Directives. Off. J. Eur. Union.

Council of the European Union, 2014. COUNCIL DIRECTIVE 2013/59/EURATOM: European Basic Safety Standards (BSS) for Protection Against Ionising Radiation.

Degering, D., Köhler, M., 2011. Gamma-spectrometric analysis of high salinity fluids – how to analyze radionuclides of the thorium decay chain far from radioactive equilibrium? Appl. Radiat. Isot. 69 (11), 1613–1617. https://doi.org/10.1016/J.APRADISO.2011.04.016.

Eggeling, L., Genter, A., Kölbel, T., Münch, W., 2013. Impact of natural radionuclides on geothermal exploitation in the Upper Rhine Graben. Geothermics 47, 80–88. https://doi.org/10.1016/J.GEOTHERMICS.2013.03.002.

Eross, A., Mádl-Szonyi, J., Surbeck, H., Horváth, Á., Goldscheider, N., Csoma, A.É., 2012. Radionuclides as natural tracers for the characterization of fluids in regional discharge areas, Buda Thermal Karst, Hungary. J. Hydrol. 426–427, 124–137. https://doi.org/10.1016/J.JHYDROL.2012.01.031.

Gallup, D.L., 1997. Aluminum silicate scale formation and inhibition: scale characterization and laboratory experiments. Geothermics 26 (4), 483–499. https://doi.org/10.1016/S0375-6505(97)00003-5.

Harmsen, K., de Haan, F.A.M., 1980. Occurrence and behaviour of uranium and thorium in soil and water. Neth. J. Agric. Sci. 28, 40–62.

Hult, M., Marissens, G., Stroh, H., Jacobsson, U., 2021. Description of the Efficiency Transfer Method Used for gamma-ray Spectrometry Activities of the RN Team at JRC Geel.

Kölbel, L., Kölbel, T., Sauter, M., Schäfer, T., Siefert, D., Wiegand, B., 2020. Identification of fracture zones in geothermal reservoirs in sedimentary basins: a radionuclide-based approach. Geothermics 85, 101764. https://doi.org/10.1016/J.GEOTHERMICS.2019.101764.

Kölbel, L., Ghergut, I., Sauter, M., Kölbel, T., Wiegand, B., 2021. Integrated approach into the characterization of the fracture network of a geothermal reservoir. Appl. Geochemistry 129, 104967. https://doi.org/10.1016/J.APGEOCHEM.2021.104967.

Kovács-Bodor, P., et al., 2019. Natural radioactivity of thermal springs and related precipitates in Gellért Hill area, Buda Thermal Karst, Hungary. J. Environ. Radioact. 201, 32–42. https://doi.org/10.1016/j.jenvrad.2019.01.020.

Krane, K.S., 1988. Introductory Nuclear Physics. Wiley, New York.

Lenntech, B.V.. Lead and water: reaction mechanisms, environmental impact and health effects. https://www.lenntech.com/periodic/water/lead/lead-and-water.htm#:~:text=Solubilityofleadandleadcompounds&text=Leadfrequentlybindstosulphur,insoft%2Cslightlyacidicwater. (Accessed 24 June 2024).

Lutter, G., Hult, M., Marissens, G., Stroh, H., Tzika, F., 2018. A gamma-ray spectrometry analysis software environment. Appl. Radiat. Isot. 134, 200–204. https://doi.org/10.1016/J.APRADISO.2017.06.045.

Mahler, A., Røgen, B., Ditlefsen, C., Nielsen, L.H., Vangkilde-Pedersen, T., 2013. Geothermal energy use, country update for Denmark. Eur. Geotherm. Congr. 3–7 [Online]. www.geotermi.dk. (Accessed 10 June 2024).

Mathews, M., Gotkowitz, M., Ginder-Vogel, M., 2018. Effect of geochemical conditions on radium mobility in discrete intervals within the Midwestern Cambrian-Ordovician aquifer system. Appl. Geochemistry 97, 238–246. https://doi.org/10.1016/j.apgeochem.2018.08.025.

Mathiesen, T., et al., 2021. PERFORM best practice for geothermal plants to minimize scaling and corrosion. https://www.geothermperform.eu/wp-content/uploads/2021/11/Best-practice-guide-for-geothermal-plants-to-minimize-scaling-and-corrosion.pdf.

Palomo-Torrejón, E., Colmenar-Santos, A., Rosales-Asensio, E., Mur-Pérez, F., 2021. Economic and environmental benefits of geothermal energy in industrial processes. Renew. Energy 174, 134–146. https://doi.org/10.1016/J.RENENE.2021.04.074.

Pauwels, J., Salah, S., Vasile, M., Laenen, B., Cappuyns, V., 2021. Characterization of scaling material obtained from the geothermal power plant of the Balmatt site, Mol. Geothermics 94, 102090. https://doi.org/10.1016/J.GEOTHERMICS.2021.102090.

Perko, T., Geysmans, R., 2023. RICOMET 2023: Managing NORM in Geothermal Installations [Workshop]. Mol.

Publication Office of the European Union, 2000. Radiological Protection Principles Concerning the Natural Radioactivity of Building Materials, p. 24 [Online]. https://op.europa.eu/en/publication-detail/-/publication/988f3243-5259-43a5-b621-fbff662deeb0/language-en. (Accessed 10 June 2024).

Regenspurg, S., et al., 2010. Geochemical properties of saline geothermal fluids from the in-situ geothermal laboratory Groß Schönebeck (Germany). Chem. Erde 70 (Suppl. 3), 3–12. https://doi.org/10.1016/J.CHEMER.2010.05.002.

Regenspurg, S., Dilling, J., Mielcarek, J., Korte, F., Schkade, U.-K., 2014. Naturally occurring radionuclides and their geochemical interactions at a geothermal site in the North German Basin. Environ. Earth Sci. 72 (10), 4131–4140. https://doi.org/10.1007/S12665-014-3306-6.

Rihs, S., Condomines, M., Fouillac, C., 1997. U- and Th-series radionuclides in CO2-rich geothermal systems in the French Massif Central. J. Radioanal. Nucl. Chem. 226 (1), 149–157. https://doi.org/10.1007/BF02063640.

Rijksoverheid, 2024. Besluit van 30 September 2024, houdende wijziging van het Besluit basisveiligheidsnormen stralingsbescherming. https://open.overheid.nl/documenten/9043fa00-e06e-4768-82ae-b7885977738e/file.

Sgs Nederland, B.V., 2020. Analytical Report SR-1993652.01.A01.

Shinonaga, T., Walther, D., Li, W.B., Tschiersch, J., 2023. Internal radiation exposure from TENORM for workers conducting cleaning activities on equipment used at geothermal energy plant. Int. J. Hyg Environ. Health 248, 114061. https://doi.org/10.1016/J.IJHEH.2022.114061.

Talvitie, N.A., 1972. Electrodeposition of actinides for alpha spectrometric determination. Anal. Chem. 44 (2), 280–283. https://doi.org/10.1021/AC60310A013.

TNO-GDN, "Formatie van Slochteren," Stratigrafische Nomenclator Van Nederland, TNO – Geologische Dienst Nederland.

Tomaszewska, B., Bodzek, M., 2013. The removal of radionuclides during desalination of geothermal waters containing boron using the BWRO system. Desalination 309, 284–290. https://doi.org/10.1016/J.DESAL.2012.10.027.

UNSCEAR, 2000. United Nations Scientific Committtee on the Effects of Atomic Radiaiton. Sources and Effects of Ionizing Radiation. New York, US.

van Bochove, L., 2023. Geothermie Nederland Industrie Standaard Geothermie NORM - Concept.

Vasile, M., Bruggeman, M., Van Meensel, S., Bos, S., Laenen, B., 2017. Characterization of the natural radioactivity of the first deep geothermal doublet in Flanders, Belgium. Appl. Radiat. Isot. 126, 300–303. https://doi.org/10.1016/J.APRADISO.2016.12.030.

Vidmar, T., 2005. EFFTRAN—A Monte Carlo efficiency transfer code for gamma-ray spectrometry. Nucl. Instruments Methods Phys. Res. Sect. A Accel. Spectrometers, Detect. Assoc. Equip. 550 (3), 603–608. https://doi.org/10.1016/J.NIMA.2005.05.055.

Zhang, T., Gregory, K., Hammack, R.W., Vidic, R.D., 2014. Co-precipitation of radium with barium and strontium sulfate and its impact on the fate of radium during treatment of produced water from unconventional gas extraction. Environ. Sci. Technol. 48 (8), 4596–4603. https://doi.org/10.1021/ES405168B/SUPPL_FILE/ES405168B_SI_001.PDF.